Opening TRPP2 (*PKD2L1*) requires the transfer of gating charges

Leo C. T. Ng[a], Thuy N. Vien[a], Vladimir Yarov-Yarovoy[b], and Paul G. DeCaen[a,1]

[a]Department of Pharmacology, Feinberg School of Medicine, Northwestern University, Chicago, IL 60611; and [b]Department of Physiology and Membrane Biology, University of California, Davis, CA 95616

Edited by Richard W. Aldrich, The University of Texas at Austin, Austin, TX, and approved June 19, 2019 (received for review February 18, 2019)

The opening of voltage-gated ion channels is initiated by transfer of gating charges that sense the electric field across the membrane. Although transient receptor potential ion channels (TRP) are members of this family, their opening is not intrinsically linked to membrane potential, and they are generally not considered voltage gated. Here we demonstrate that TRPP2, a member of the polycystin subfamily of TRP channels encoded by the *PKD2L1* gene, is an exception to this rule. TRPP2 borrows a biophysical riff from canonical voltage-gated ion channels, using 2 gating charges found in its fourth transmembrane segment (S4) to control its conductive state. Rosetta structural prediction demonstrates that the S4 undergoes ∼3- to 5-Å transitional and lateral movements during depolarization, which are coupled to opening of the channel pore. Here both gating charges form state-dependent cation–π interactions within the voltage sensor domain (VSD) during membrane depolarization. Our data demonstrate that the transfer of a single gating charge per channel subunit is requisite for voltage, temperature, and osmotic swell polymodal gating of TRPP2. Taken together, we find that irrespective of stimuli, TRPP2 channel opening is dependent on activation of its VSDs.

ion channels | biophysics | TRP channels | gating mechanisms | polycystins

Ion channels control the flow of ions across membranes and are required for short- and long-range electrical signaling (1). Voltage-gated ion channels (VGICs) are characterized by their ability to turn on the flow of ionic current by opening their conductive pore in response to changes in membrane potential. Typically, each VGIC subunit has 6 transmembrane segments (S1 to S6) which oligomerize to form an ion channel as a homotetramer. Each of the 4 subunits is domain swapped, where the S5 and S6 from each subunit form the ion conducting pore domain (PD) which are flanked by a 4-helix bundle (S1 to S4) called the voltage sensor domain (VSD) (2–4). Voltage-dependent opening or gating of VGICs is tightly controlled by the up or down state (activated or deactivated) of the S4 transmembrane segment (5, 6). When the cell membrane is depolarized, the opening of the PD is mechanically linked to conformational changes in the S4 through physical interactions between the S4–S5 linker and the S6 helix (7, 8). In the quaternary channel structure, the activation of the VSDs is coupled to a concerted 4-fold displacement of the S6 cytosolic gate, which dilates the PD enough to allow the passage of ions (3, 9). There are typically 4 highly conserved positively charged residues (arginine or lysine), called "gating charges," at every third amino acid position within the S4 (6, 10). Based on structural, computational, and functional studies, these gating charge residues form sequential stabilizing electrostatic bonds within the VSD which catalyze the S4 segment's outward translocation in response to membrane depolarization (11–13).

Within the VGIC superfamily, the gating mechanisms of transient receptor potential (TRP) channel class are unique among the 6 subclasses (A, C, M, ML, P, and V) (14). TRP channels perform sensory functions for the cell, opening in response to diverse stimuli such as temperature shifts and binding of chemical ligands, which are often defining features of each subclass (15). Here the energy of association between most TRP channels and their ligands (exogenous or endogenous) is sufficient to initiate channel opening. Although TRP channels share a similar topology with most VGICs, few are intrinsically voltage gated, and most do not have gating charges within their VSD-like domains (16). Current conducted by TRP family members is often rectifying, but this form of voltage dependence is usually attributed to divalent block or other conditional effects (17, 18). There are 3 members of the polycystin subclass: TRPP1 (PKD2 or polycystin-2), TRPP2 (PKD2-L1 or polycystin-L), and TRPP3 (PKD2-L2). TRPP1 is the founding member of this family, and variants in the PKD2 gene which encode this channel are associated with autosomal dominant polycystic kidney disease (ADPKD) (19). Homomeric forms of TRPP1 do not form functional channels on the plasma membrane when expressed either heterologously or endogenously (20). Rather, TRPP1 localizes and functions exclusively in the membranes of primary cilia and ER organelles, which presents a significant challenge to studying their gating behavior (21–23). TRPP2 also localizes to the primary cilia of several nonrenal cells but differs from TRPP1 because it forms an ion channel in the plasma membrane as well (24). This localization feature facilitates the present study, where gating behavior of TRPP2 and voltage sensor function is assessed in plasma membranes under overexpressed conditions. The structures of TRPP1 and TRPP2 in closed and ion occupied states have been reported, but our understanding of the intramolecular interactions responsible for channel gating is largely undefined (20, 25–28). Here we ask, what is the molecular mechanism responsible for this channel's voltage dependence? We have determined that opening of TRPP2 requires the transfer of a single gating charge per subunit, as

Significance

Dysfunction of polycystin TRP channels (TRPPs) is associated with polycystic kidney disease (PKD), but their biophysical and structural regulation is poorly understood. We report that TRPP2 voltage sensor activation is required to open the conducting pore, regardless of polymodal stimuli. Each of the 4 voltage sensor domains delivers at least 1 gating charge prior to TRPP2 channel opening while forming state-dependent cation–π interactions. Since these interacting positions are conserved among voltage-gated ion channels, we propose that this canonical gating mechanism was preserved during TRPP2 evolution. Our results provide a structural framework for understanding the regulation of TRPP2 in cilia and plasma membranes.

Author contributions: L.C.T.N., T.N.V., V.Y.-Y., and P.G.D. designed research; L.C.T.N., T.N.V., V.Y.-Y., and P.G.D. performed research; L.C.T.N. contributed new reagents/analytic tools; L.C.T.N., T.N.V., V.Y.-Y., and P.G.D. analyzed data; and T.N.V. and P.G.D. wrote the paper.

The authors declare no conflict of interest.

This article is a PNAS Direct Submission.

[1]To whom correspondence may be addressed. Email: paul.decaen@northwestern.edu.

This article contains supporting information online at www.pnas.org/lookup/suppl/doi:10.1073/pnas.1902917116/-/DCSupplemental.

Published online July 17, 2019.

measured directly in the form of gating current. These capacitive currents are carried by residues K452 and K455 in the S4 segment which are conserved gating charge positions in VGICs. In conjunction with Rosetta structural modeling and the recently resolved polycystin structures, we find Y366 in the S2 segment is energetically coupled to the S4 gating charges through the formation of cation–π interactions. Based on our modeling of TRPP2 gating, the S4 segment undergoes both translational and lateral movements as the sensor activates. The activation of the S4 is coupled to the ∼7.6-Å radial dilation of the 4 S6 helices that form the intracellular gate, which opens the ion conducting pathway. Like most TRP channels, TRPP2 gating is polymodal, and stimuli such as membrane tension or thermal energy potentiate its ionic current. Importantly, we find that TRPP2 cannot open using these stimuli is unless both gating charges are intact. Our results demonstrate that gating charge transfer and activation of the VSD are necessary steps in TRPP2 channel opening. These results define how TRPP2 integrates these stimuli in conjunction with membrane potential to control the flow of calcium and monovalent cations into the cell through cilia and plasma membranes.

Results

TRPP2 and VGICs Share a Voltage-Dependent Gating Mechanism. A cardinal feature of voltage-gated channels are large tail currents activated by membrane repolarization, which capture the ion flow during the transition from the open to closed states in the whole-cell patch configuration. This feature is not commonly found in TRP channels; however, we and several groups have previously shown that TRPP2 is an exception (29–31). In the symmetrical sodium conditions devoid of divalent ions, whole-cell patched HEK293T cells overexpressing this channel generate robust tail currents upon repolarization and can be fit to a Boltzmann function (*SI Appendix*, Fig. S1*A*). The half-maximal voltage dependence of TRPP2 activation is positive ($V_{1/2}$ = 47 mV), and the slope of the current voltage relationship is shallow (Z = 1.1), which infers a transfer of approximately 1 gating charge per channel subunit (*SI Appendix*, Table S1). Based on these functional characteristics, we hypothesized that TRPP2 channel proteins likely contain a voltage sensing element. Several high-resolution structures of TRPP1 and TRPP2 have been determined by single partial cryo-EM (20, 25–28), and their conserved S4 lysines (K452 and K455 in TRPP2) structurally align to the third and fourth gating charge positions

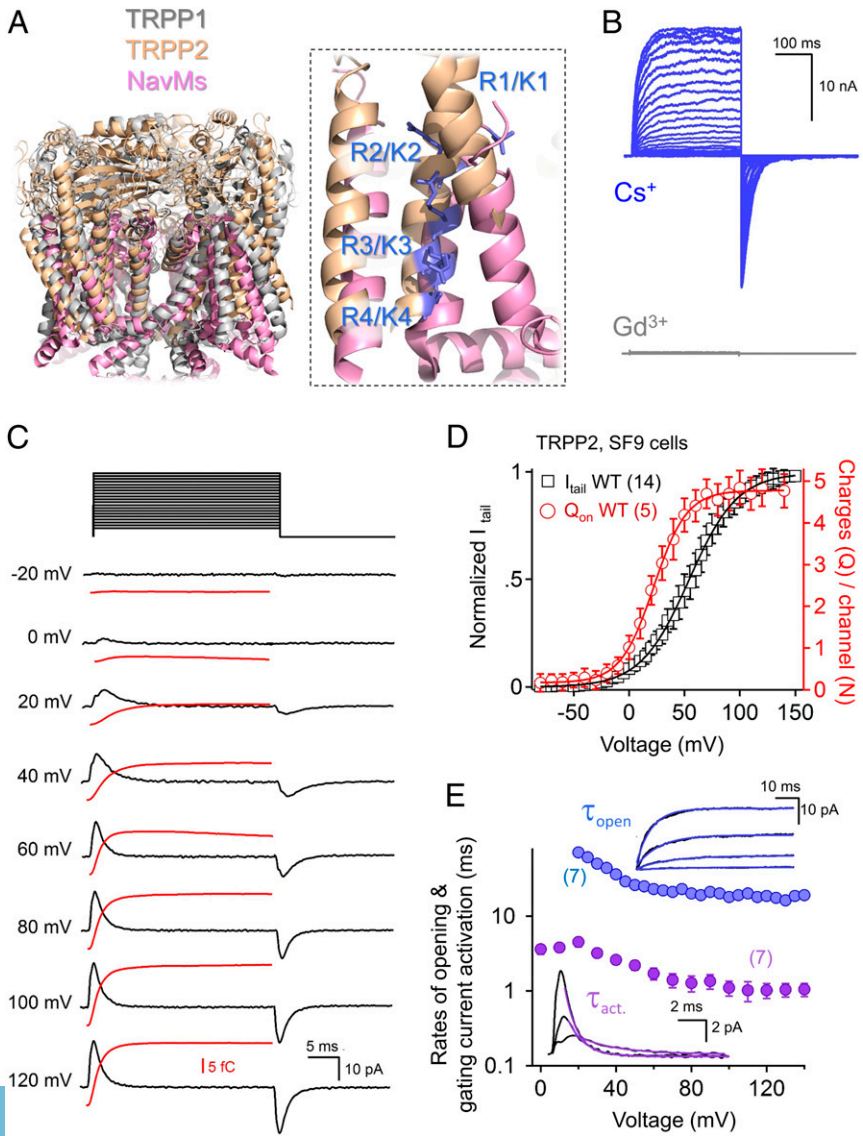

Fig. 1. Gating currents generated by gating charges in TRPP2's voltage sensor. (*A*) A structural alignment of TRPP1, TRPP2, and the prokaryotic voltage-gated sodium channel NavMs (PDB accession codes 5T4D, 5Z1W, and 5HVX, respectively) (7, 20, 26). (*Right*) Expanded view of the VSD helices. Note the conserved gating charge positions R3/K3 and R4/K4 from TRPP2 and NavMs. (*B*) Steady-state voltage-dependent Cs^+ currents (blue traces, *Top*) recorded from SF9 insect cells and blocked Gd^{3+} (gray traces, *Bottom*). (*C*) HA-TRPP2-GFP gating currents (black traces) activated by voltage steps shown above. The integrated gating currents (red) convert from current to charge (femtocoulombs [fC]). (*D*) The voltage dependence of the central pore tail current (black) and the estimated charges per channel (red), fit to the Boltzmann equation. (*E*) A comparison of the rates of central pore current opening (τ_{open}) and gating charge activation (τ_{act}). Number replicates are indicated in the parentheses, and error bars are SEM.

found in canonical potassium (K_v) and sodium (Na_v) VGICs (Fig. 1*A*). Interestingly, among the 4 gating charge positions—which can be lysine (K1 to K4) or arginine (R1 to R4)—the innermost buried charges K3 and K4 are the most conserved in the VGIC superfamily (*SI Appendix*, Fig. S1*B*). For simplicity, the K/R1 to K/R4 nomenclature is used for the remainder of this manuscript when referring to these gating charge positions. Thus, because of their alignment along the S4 and the clear voltage dependence of this channel, we hypothesize that K3 and K4 are involved in voltage-dependent gating of TRPP2 channels.

Next, we asked, what is the functional impact of neutralizing the present gating charges (K3 and K4)? In TRPP2, neutralization of either K3 or K4 to 1 of 6 amino acids (A/C/D/H/Q/I) completely ablates the tail currents. However, when the positively charged side chain is preserved with an arginine substitution, the tail currents from TRPP2 K3R and K4R channels are restored (*SI Appendix*, Fig. S1*C*). While there is a small shift in the $V_{1/2}$ of K3R and K4R by 13 and 2 mV, respectively, the mutations do not change the transfer of a single apparent charge (*SI Appendix*, Table S1). Apparently, the positive nature of the side chain at K3 and K4 is essential for TRPP2 voltage-dependent gating. In contrast to TRPP2, the voltage dependences of canonical VGICs are typically negative ($V_{1/2}$ = −5 to −50 mV), and their apparent charge based on the slope is steep (Z = 2.5 to 4.6). Thus, we hypothesized that TRPP2 voltage dependence could be reproduced in VGICs by only removing the first 2 gating charges (K1 and K2), leaving only K3 and K4 intact as they are found in TRPP2. To test this, we selected the NaChBac prokaryotic VGIC, whose gating current and voltage-dependent properties have been extensively characterized (12, 32, 33). Here we neutralized the 2 most extracellular gating charges (R1Q:R2Q) and observed a shift in its $V_{1/2}$ from −34 to 45 mV and a reduction in its apparent charge transfer (Z) from 3.7 to 1.1 compared with the Wt channels (*SI Appendix*, Fig. S2 *A* and *B* and Table S1). Thus, voltage-dependent parameters of the NaChBac R1Q:R2Q channel closely resemble TRPP2. These data suggest that TRPP2's positive and shallow voltage dependence is a product of having only 2 gating charges in its voltage sensor, a feature that can be recapitulated in a canonical VGIC simply by reducing the number of gating charges from 4 to 2. However, additional glutamine neutralization of either R3 (R1Q:R2Q:R3Q) or R4 (R1Q:R2Q:R4Q) abolishes channel function without impacting its membrane localization (*SI Appendix*, Fig. S2*C*). Based on these observations, we conclude that K/R3 and K/R4 are essential gating charges to TRPP and VGIC gating.

TRPP2 Channels Generate Gating Current Which Is Dependent on S4 Gating Charges. TRPP2 has a shallow voltage dependence (Z = 1.1) which implies the transfer of a single gating charge per channel subunit. However, this is an indirect measurement, and we sought to directly measure the gating charge transfer from TRPP2 using the previously established Q/N method (34, 35). The measurement of gating current requires the high expression of channels because it is an order of magnitude smaller than central pore current. To achieve this, we overexpressed HA-TRPP2-GFP channels in SF9 insect cells using a baculovirus to enhance the number of channels beyond the levels obtainable in HEK cells. To estimate the total number of channels (N), we measured the single-channel conductance (γ), open probability (Po), and whole-cell current (I_{wc}) (Fig. 1*B* and *SI Appendix*, Fig. S3 *B*–*D*). Here we used Cs^+ as a charge carrier because K^+ and Na^+ currents saturated the amplifier in nearly every cell clamped, prohibiting the estimation of the total I_{wc} due to their high conductance through the TRPP2 channel (*SI Appendix*, Fig. S3*A*). We calculate an average of 29,734 channels per insect cell using the above parameters (γ, Po, I_{wc}; *SI Appendix*, Table S2). As expected, TRPP2 currents measured from insect cells are outwardly rectifying with similar voltage dependence ($V_{1/2}$ = 55 mV) and tail current kinetics (τ_{close} = 20 ms) to those measured from HEK cells (*SI Appendix*, Tables S1 and S2). We then blocked the central pore current by removing the permeant ion and adding the trivalent pore-blocker Gd^{3+} (Fig. 1*B*). Then, we measured capacitive gating currents activated by voltage steps from a −100-mV holding potential (Fig. 1*C*). The gating currents were integrated from each voltage step to establish the half maximal gating charge–voltage relationship (Q_{on}). Here the Q_{on} for TRPP2 was 22 mV, which is 23 mV more negative than the voltage required to open of the central pore current (Fig. 1*D*). After dividing the maximum gating charge by the number of channels, we estimate that the complete activation of each TRPP2 channel involves the transfer of 4.7 charges per channel, or 1.1 charges per each of the 4 TRPP2 subunits. We compared the opening rate of the ionic pore current (τ_{open}) to the activation rate of the gating charges ($\tau_{act.}$) and observed that the voltage sensor charges activate 8 to 10 ms faster than the opening of the central pore (Fig. 1*E*). Gating charge transfer measured VGICs typically exhibit charge immobilization after prolonged depolarization (36). To determine if TRPP2 channels exhibit this feature, we held the membrane potential at +60 mV and stepped to negative potentials to capture the deactivation charge (Q_{off}) of the integrated inward gating currents (*SI Appendix*, Fig. S4*A*). Here the corresponding voltage dependence was shifted by −19 mV, suggesting that TRPP2 gating charges were immobilized by the prolonged depolarization (*SI Appendix*, Fig. S4*C* and Table S2). Taken together, these data suggest that the TRPP2 VSD activation before pore opening along the temporal and voltage scales is a sequence of events that is shared by VGICs (32, 37). Finally, the gating charge measurement and central pore currents were completely abolished when either K3 or K4 gating charges were neutralized to glutamine (*SI Appendix*, Fig. S4 *B* and *C*). Importantly, neither K3Q nor K4Q mutations altered the plasma membrane localization levels in insect cells, as assessed by live cell imaging of colocalized HA-TRPP2-GFP with plasma membrane labeling and surface protein biotinylating (*SI Appendix*, Fig. S4 *C* and *D*). Hence, preservation of charges at the K3 and K4 positions is necessary for gating charge transfer, the first mechanistic step in opening TRPP2.

TRPP2 Gating Charges Form Interactions within the VSD During Activation. The classic and consensual view of voltage-dependent gating of VGICs proposes that the S4 segments move up in response to membrane depolarization. The movement of the S4 is accompanied by rearrangements within the VSD, which exposes gating charges to a water-filled cavity on the extracellular side. During this transition, the gating charges form stabilizing hydrogen bonds and salt bridge interactions with intervening side-chain and carbonyl oxygens from the other VSD helices S1 to S3. We hypothesized that the S4 of TRPP2 VSD might take a similar trajectory. As identified in the initial reports of TRPP1 and TRPP2 channel structures, the hydroxylphenylalanine group of S2-Y366 faces the ε-ammonium group of K3 and K4, which are separated by ∼5 Å (Fig. 2*B*) (20, 26). Thus, we proposed that the gating charges may form cation–π or hydrogen bond interactions with Y366 during VSD activation. First, we calculated the perturbation in free energy of channel opening (ΔG°) caused by single point mutations. We observed 21- to 30-mV shifts in the $V_{1/2}$, which in turn increased the ΔG° by 0.8 to 1 kcal/mol for the K3R, K4R, and Y366F single mutants compared with Wt channels (Fig. 2*A* and *SI Appendix*, Table S1). Next, as qualitative support for the interactions, we applied the double-mutant cycle analysis method to determine if these positions are energetically coupled (ΔΔG°) during TRPP2 gating (*SI Appendix*, *Material and Methods*) (9). We determined there are −1.5 and −0.5 kcal/mol of coupled free energy (non-additive) for the K3R-Y366F and K4R-Y366F interacting pairs,

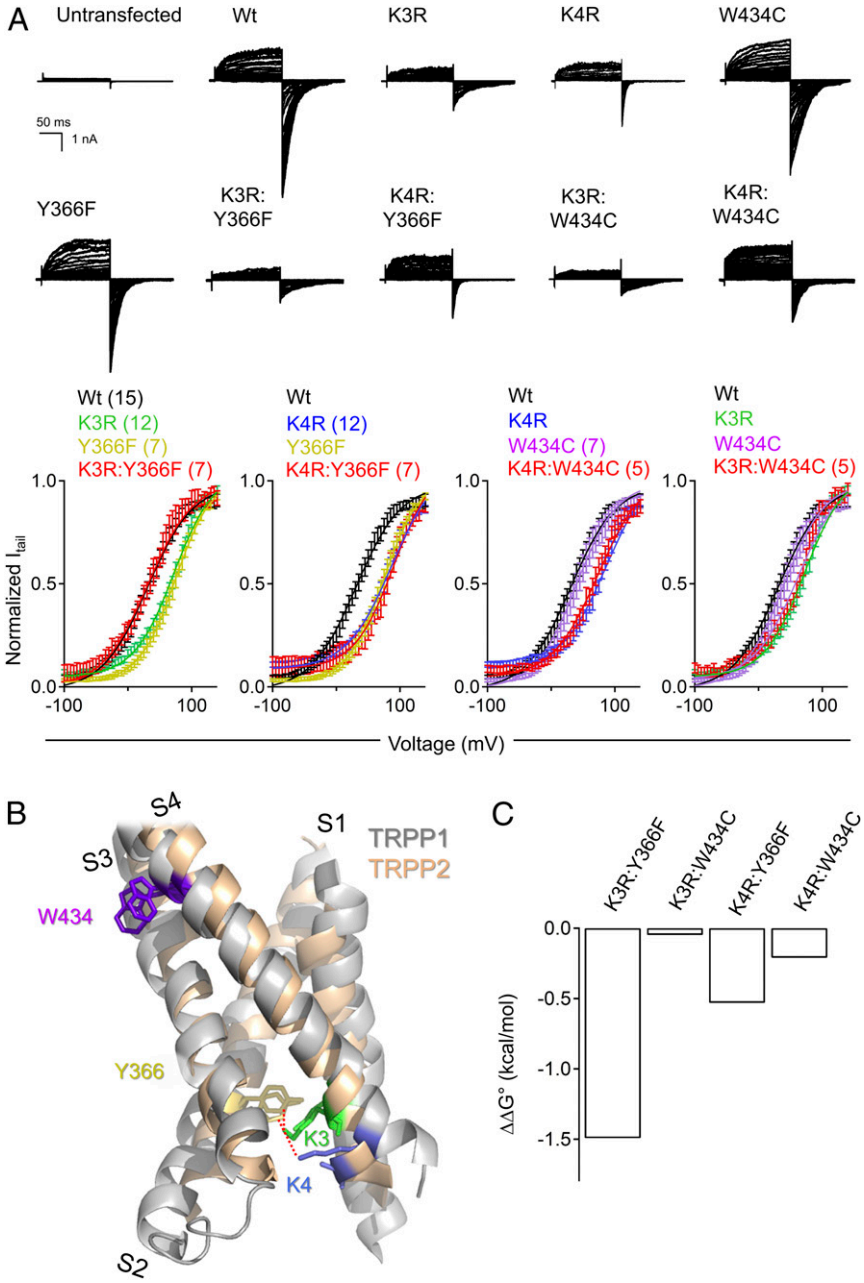

Fig. 2. Mutant cycle analysis reveals coupling energy between gating charges and Y366F. (*A*) (*Top*) Steady-state voltage-dependent currents from single- and double-mutant TRPP2 channels recorded from HEK cells, with the same protocol shown in Fig. 1*A*. (*Bottom*) Resulting normalized tail current shown as current–voltage relationship from proposed interacting pairs. (*B*) Structural locations of the proposed interacting (red dotted line) and noninteracting residues within the TRPP2 voltage sensor. (*C*) The amount of nonadditive or coupled free energy (ΔΔG°) from 4 pairs cycle analyzed (*SI Appendix, Methods*).

respectively (Fig. 2*C*). As a negative control of our cycle analysis, we chose W434, which is located at the top of S4 facing away from the center of the VSD helix bundle and thus is unlikely to interact with gating charges K3 and K4 during the activation process (Fig. 2*B*). As expected, the couple energy for K3R-W434C and K4R-W434C were additive ($\Delta\Delta G° < 0.25$ kcal/mol), which suggests that neither gating charge interacts with W434 during the opening of TRPP2 (Fig. 2 *A* and *C* and *SI Appendix*, Table S1). Based on the TRPP2 structures (26, 27), other sites within the VSD such as Y107 of the S1 segment and D390 of the S3 segment may also interact with the gating charges, but recordings from cells expressing mutations at these positions did not yield current above background levels.

Thus far, we have shown that TRPP2 generates gating currents that are dependent on gating charges and that these residues likely interact with Y366 during activation of the VSD. However, does the TRPP2 VSD undergo voltage-dependent conformational changes as reported for VGICs? Based on the TRPP2 structures, the side chain of H404 in S3 faces the VSD gating pore which might become solvated by extracellular water in the activated state (Fig. 3*A*). We generated the H404C channel mutant and tested for current modification by extracellularly applying 2-sulfonatoethyl-methanethiosulfonate (MTSES), a negatively charged (cell impermeant) cysteine thiol modifying agent. Here we observe rapid antagonism ($\tau = 230$ ms $\pm$ 73) of the H404C tail current, whereas the Wt current was unaffected upon MTSES

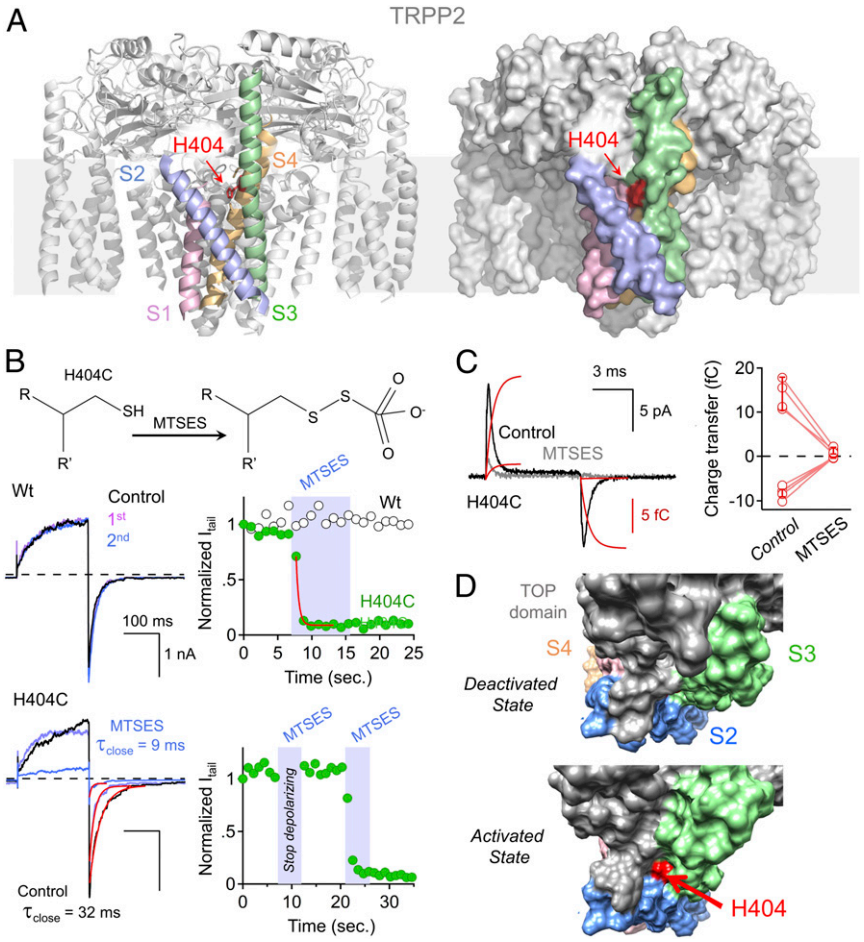

Fig. 3. MTSES modification of H404C is state dependent. (*A*) Transmembrane views of the TRPP2 channel structure, showing H404 (red) side chain is exposed and accessible in the up state. (*B*) (*Top*) Reaction scheme of H404C thiol modification by 30 μM MTSES. (*Bottom Left*) Currents from Wt and H404C channels activated by a 0.2-Hz train of 100-mV depolarizations. (*Bottom Right*) The time course of normalized tail current magnitudes before and after 30 μM MTSES modification (blue shaded regions). The decay in tail current is only observed with the cysteine substitution and if MTSES is applied when the VSD is activated. (*C*) (*Left*) H404C TRPP2 gating currents before (black traces) and after cystine modification (gray traces) with MTSES. Gating currents were activated by depolarizing the membrane potential to 60 mV from a holding potential of −100 mV. (*Right*) Inward and outward gating charge transfer measured before and after MTSES modification. Four cells expressing the H404C channel were tested, and the error bars are equal to SD. (*D*) Extracellular view of the Rosetta structural model of the TRPP2 VSD. Note the displacement of the TOP domain by the S3 during transition from the deactivated (*Top*) to activated (*Bottom*) states and the accessibly of H404 (red) from the extracellular side in the activated state.

application (Fig. 3*B*). Next, we asked, is MTSES modification of this site dependent on activating the voltage sensor? We held the sensor in the deactivated state (or down state) and the channel pore closed by clamping the membrane potential at −100 mV (without depolarizing) while applying MTSES extracellularly (Fig. 3*B*). After withdrawing the MTSES, we activated the channels using depolarizing ramps and observed no change in the current magnitude from the control condition. However, from the same cell, when we activated the channel in the presence of MTSES, the current rapidly decayed. The current did not return upon withdrawal of the MTSES agent, a result consistent with covalent modification of the cysteine sulfhydryl. We observed that the rate of channel closure—given by the time constant of the tail current—was enhanced ∼3× when H404C was MTSES-modified (control τ_{close} = 32 ms and MTSES τ_{close} = 9 ms). To determine if the MTSES-induced reduction in ion current was due to VSD modification, we measured Q_{on} from H404C and observed a 92% reduction after applying MTSES (Fig. 3*C*). These observations suggest that the MTSES negative charge modification of H404C neutralizes the positive gating charges or disrupts gating charge transfer during VSD activation. Regardless of interpretation, the VSD clearly undergoes conformational changes which expose the buried H404 residue to the aqueous environment when the sensor is activated. In the next section, we use the Rosetta method to model the state-dependent molecular interactions supported by our functional assays and to predict how the voltage sensor controls the opening of the TRPP2 pore.

Modeling of TRPP2 Voltage Sensor Activation and Channel Opening Using Rosetta. We used Rosetta structural modeling to predict TRPP2 conformational changes during channel gating using cryo-EM structures of TRPP1 and TRPP2 templates as described in our methods (20, 25–28). The S4–S5 linker region in the TRPP2 open state model was predicted de novo because the corresponding region was unresolved previously (26). There are few global differences in the TOP domain, whereas the greatest differences were observed in the VSD and PD between the modeled open and closed states. Within the VSD, the S4 segment moves transitionally and laterally by ∼3 to 5 Å, and the S4–S5 linker moves laterally by ∼16 Å N-terminally and by ∼2 Å C-terminally (Fig. 4*A*). The Cα atoms of the gating charge residues K3 and K4 in S4 segment move in the plane of the membrane by ∼3.6 and ∼5.4 Å, respectively (Fig. 4*B* and Movie S1). In this model, 2 electrostatic interactions in the VSD help

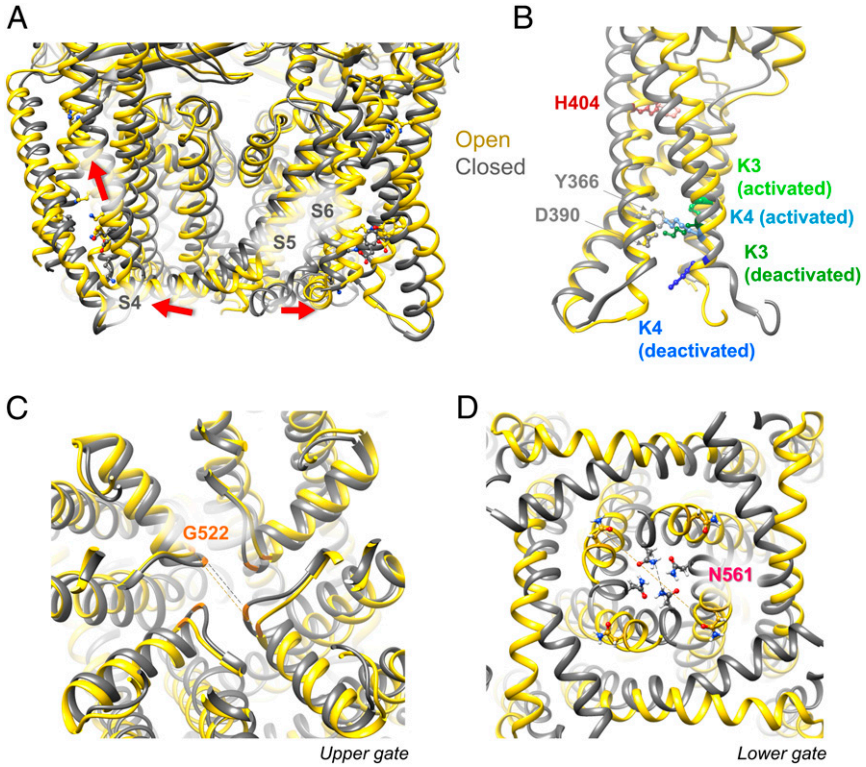

Fig. 4. Rosetta model of TRPP2 in the open and closed states. (*A*) A transmembrane view of the open (yellow) and closed (dark gray) TRPP2 channel models. The arrows depict the conformational changes expected to occur in 1 TRPP2 protomer during channel opening. The S4 segment translates upward during voltage sensor activation, shifting the gating charges K3 (green) and K4 (blue). The de novo predicted S4–S5 linker in the open state also shifts compared with the closed state as a result. Finally, the S6 moves laterally away from the central pore, allowing the opening of the lower gate in D. (*B*) The gating charges K3 and K4 form sequential cation–π interactions with the gating charge transfer center Y366 when the voltage sensor is activated. S3 residue H404 (red) does not change significantly between the predicted states. (*C*) An extracellular view of the channel pore in the open and closed states. Residue G522 forms the putative upper gate and dilates by 2.7 Å when the channel opens. (*D*) An intracellular view of the channel pore and the lower gate. The narrowest point in the lower gate, N561, widens by 7.6 Å when TRPP2 opens.

stabilize the gating charges during voltage sensor activation. Interestingly, the highly conserved negatively charged D390 of S3 segment stabilizes K3 in the closed state and K4 in the open state. Because these positions are conserved in the TRPP1 channels, this interaction is likely disrupted by the ADPKD-causing D511V variant (*Discussion*). Our model predicts that the ammonium side chain of K4 only forms a cation–π interaction with Y366 in the open state but not the closed state. These interactions are supported by the coupling energies measured between the gating charges and Y366 (Fig. 2*C*). Here the S4 segment undergoes an upward helical turn, transferring the side chain of K3 from below to above the Y366 hydroxyphenylalanine side chain when the VSD is activated (Fig. 4*B*). Thus, based on this model, K3 appears to be the site responsible for delivering the observed 1.1 gating charges per channel subunit during channel activation. After the VSD activates, the PD of TRPP2 opens. Based on the reported TRPP2 channel structure, the pore was proposed to have an intracellular and an extracellular gate. The extracellular gate, which is formed by G522 near the selectivity filter, only dilates by ~2.7 Å during the transition from the closed to open states in our models (Fig. 4*C*). In contrast, a much larger transition was observed in the intracellular gate, which is formed by N561 in the S6. Here movement of the S4–S5 linker is coupled to a 16° rotation and 4-fold ~8 Å splay of N561 Cα atoms to open the lower gate and allow for the conduction of cations (Fig. 4*D* and Movie S2). On the extracellular side of the channel, the vertical transition of the S3–S4 during VSD activation causes structural changes in the external TOP domain (Fig. 3*D*). Here the TOP domain shields part of the VSD from the extracellular environment in the deactivated/closed state. When activated, the H404 side chain becomes exposed to the aqueous environment, a feature that likely explains the state-dependent accessibly of H404C to MTSES modification (Fig. 3*D* and Movie S3).

Gating Charge Transfer Is Required to Polymodally Activate TRPP2. The half maximal activation of TRPP2 is 47 mV, which is outside the physiological range of membrane potentials experienced by most cells. Thus, we wondered if other polymodal stimuli may enhance channel opening by shifting its voltage dependence to more negative membrane potentials. TRPP2 channels are expressed in the apical processes and primary cilia of osmotically active cells such as type III taste bud cells, spinal cord contacting neurons, and retinal pigmented epithelium, where its open probability is increased under high membrane tension (≥40 mmHg of membrane pressure) (24, 38, 39). However, it is not known how this stimulus activates TRPP2. First, we compared TRPP2 whole-cell currents in isotonic internal and external solutions and after shifting the extracellular osmolarity to 240 mOs to swell the cell (Fig. 5*A*). Here we observed a gradual increase in the TRPP2 outward peak and inward tail current triggered by voltage ramps over a 3-min time course which correlated with ~2.5× expansion of the cells volume. When measured in the on-cell configuration, osmotic-induced membrane swell causes an increase in the number of open channel events and mean open time without altering the single-channel conductance (*SI Appendix*, Fig. S5 *B* and *C*). These results suggest swell induction increases the time TRPP2 spends in the open state but not the efficiency of ionic charge moving through conductive pore (γ). Next, we compared the steady-state voltage

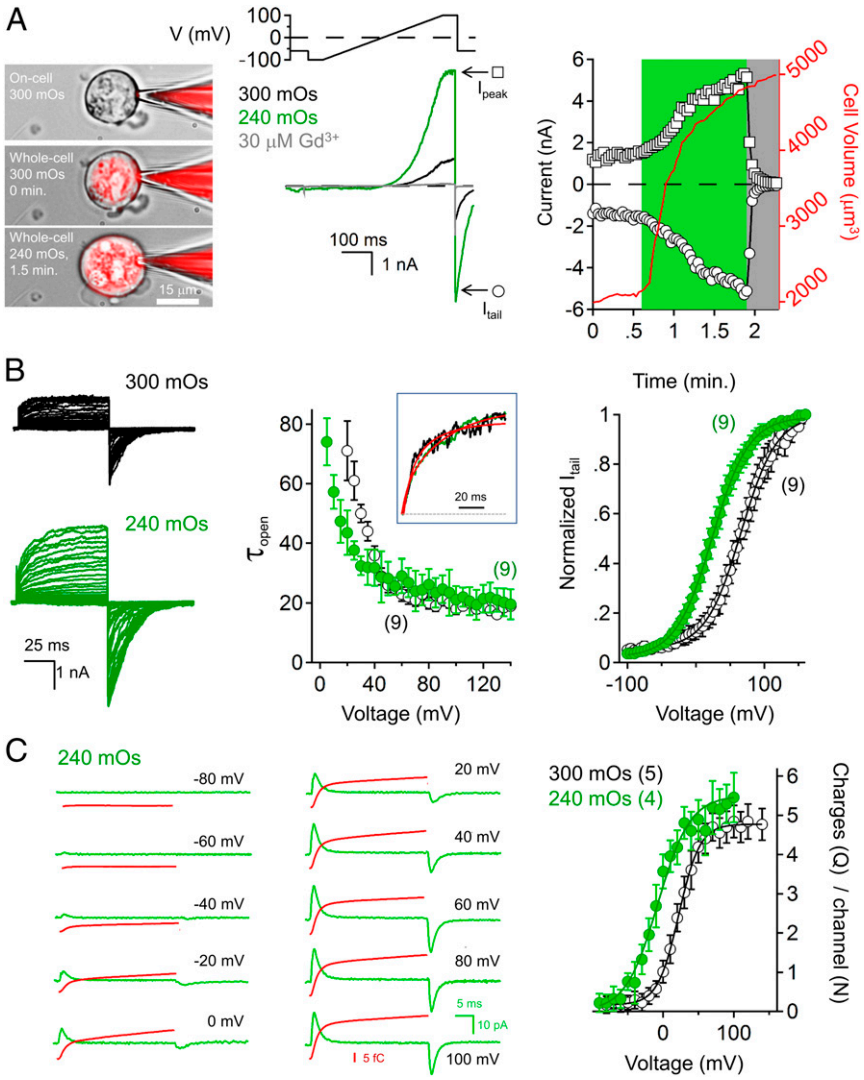

Fig. 5. Osmotic swell potentiation of TRPP2 is dependent on gating charge transfer. (*A*) The onset of the TRPP2 current potentiation and swelling of the cell membrane. (*Left*) Images of a patch clamped SF9 insect cell in the on-cell configuration, the whole-cell configuration, and after swelling the membrane by decreasing the external osmolarity (240 mOs). The pipette was filled with standard internal saline and 30 nM Alexa Fluor 588 (red color; Invitrogen) to visualize the continuity between electrode and the volume of the intracellular compartment while the cell swelled in response to lowering the external osmolarity. (Scale bar, 15 µm.) (*Middle*) TRPP2 currents activated by a 0.2-Hz train of voltage ramps before and after membrane swell. Note that the outward (I_{peak}) and inward (I_{tail}) currents are antagonized by the TRPP2 channel antagonist 30 µM Gd^{3+}. (*Right*) The time course of the increase in cell volume (red) and the onset of TRPP2 current potentiation. (*B*) (*Left*) Exemplar steady TRPP2 whole-cell currents activated before and after membrane swelling. (*Middle*) Rate of channel opening is estimated by the onset of current rise time. (*Inset*) Exemplar currents from the normal and swell conditions. (*Right*) Resulting normalized tail currents demonstrating the shift in the voltage dependence of activation. (*C*) (*Left*) Exemplar gating current (green) and integrated current (red) traces measured after blocking the central pore current with Gd^{3+} and osmotically swelling the cell membrane. (*Right*) Corresponding estimate of gating charges per channel and membrane voltage relationship. Note the −28-mV shift in $QV_{1/2}$ after 240 mOs membrane swelling (green circles, $QV_{1/2}$ = −6 mV) compared with the 300 mOs isotonic condition (white circles, $QV_{1/2}$ = 22 mV).

dependence before and after swelling the TRPP2-expressing SF9 cells. We observed a −38-mV shift in $V_{1/2}$ and a small decrease in the closure rate but no change in the fit of the Boltzmann curve slope, suggesting that TRPP2's sensitivity to voltage was enhanced but the amount of apparent gating charge transfer (Z) remained the same after swelling the cell (Fig. 5*B* and *SI Appendix*, Fig. S5*B* and Table S2). As we had done previously, we blocked the central pore current using Gd^{3+} and measured gating currents before and after membrane swelling. We also observed a −28-mV shift in $Q_{1/2}$ which was proportionally shifted relative to the $V_{1/2}$ of the central pore current (Fig. 5*C* and *SI Appendix*, Table S2). Importantly, we observed little difference in the maximum gating charge transfer (5.3 ± 0.8 charges per channel) after swelling the membrane, suggesting that the maximum amount of gating charges transferred was the same. These data demonstrate that membrane swell acts as positive modifier of the TRPP2 voltage dependence, specifically shifting the voltage sensitivity of the gating charge transfer, which increases the open probability of TRPP2 at negative membrane potentials.

Finally, we asked whether swell or heat stimuli can activate TRPP2 channels independently of a functional voltage sensor. However, we did not observe any macroscopic current from cells expressing the gating charge variants K3Q and K4Q before or after osmotic swell (*SI Appendix*, Fig. S5*A*). These data demonstrate that a functioning voltage sensor is essential for TRPP2 channel gating and that the channel pore cannot be opened independently through membrane swelling. Besides osmotic membrane swell, heat is another stimulus that polymodally

potentiates polycystin channel currents. Currents carried by homomeric TRPP2 and heteromeric TRPP2+PKD1-L1 channels are potentiated by heat when expressed in the cilium (temperature coefficient $Q_{10} = 8$) and plasma membranes ($Q_{10} = 6$) (24, 40). We wondered if heat might alter TRPP2 voltage-dependent gating as a mechanism for the observed effect. Consistent with our previous findings, we observed potentiation of the TRPP2 whole-cell currents when the bath temperature was raised (*SI Appendix*, Fig. S6*A*) (24). In addition, the 22 °C to 32 °C transition enhanced the rate of channel opening (τ_{open}) by ~ 9× and closure (τ_{close}) by ~ 10× (*SI Appendix*, Fig. S6 *B* and *C*). However, after comparing the steady-state TRPP2 currents, the increase in temperature only minimally shifted its voltage dependence of activation ($\Delta V_{1/2} = -11$ mV) and by itself is not a sufficient means to explain TRPP2's large temperature coefficient (*SI Appendix*, Fig. S6*B*). Thus, we conducted single-channel recordings and observed an increase in the unitary single-channel conductance (163 to 209 pS), consistent with reports using the mouse ortholog of TRPP2 (*SI Appendix*, Fig. S6*D*) (40). Since ion conductance is a property of the channel pore and not the voltage sensor, we tested if the TRPP2 channel can be gated independently of a functioning voltage sensor. We recorded from cells expressing the gating charge variants (K3Q and K4Q) and found that heat fails to open channels when measuring the total plasma membrane current (*SI Appendix*, Fig. S6*A*). Taken together, these finding support the inescapable conclusion that opening TRPP2 channels by swell, temperature, and membrane potential requires the initial transfer of gating charges.

Discussion

VGICs and TRPP2 Channel Opening Requires Activation of the VSD. VGICs open their ion conducting pores in response to changes in membrane potential. This conformational change is preceded by movement of 3 to 4 gating charges from each of their S4 voltage sensors—a step that is crucial for their regulation of electrical impulses in excitable cells (6). Most TRP channels have a low open probability with voltage stimulation alone and require specific ligand interactions or other stimuli to fully open. Structural analysis of TRPV, TRPM, TRPA, and TRPML channels suggest that their VSD-like domains form ligand binding sites but the S4 remains relatively static during activation (41–45). For several TRP channel subtypes, the biophysical mechanism of current rectification is achieved through extrinsic mediators, like divalent cation block of TRPM7 (17, 18). Thus, in general, members of the TRP channel families are not considered intrinsically voltage sensitive. In this paper, we show that TRPP2 channels (and possibly TRPP1) are intrinsically regulated by membrane potential through the function of 2 crucial gating charges (K3 and K4). For TRPP2, activation of the VSD appears to be the rate-limiting step and requisite for channel opening, regardless of polymodal stimuli. Results from our Rosetta modeling of TRPP2 channel in open and closed states in conjunction with our functional data support a model of polycystin opening that shares hallmark structural features found in VGICs. The consensus view of VGIC gating adopts structural features of the previously proposed transporter and sliding helix models (46, 47). The VSD undergoes voltage-dependent rearrangements where the S4 segment translocates 3 to 8 Å across the membrane electric field, and gating charges form stepwise counter charge and hydrogen bond interactions between polar and electronegative residues of the VSD (11, 13). At the same time, water-exposed crevasse within the VSD is formed on extracellular side of the membrane, where previously buried residues are exposed to the aqueous environment when the sensor is activated (48).

We directly measured the transfer of 4.5 gating charges per TRPP2 channel (or ~1.1 charge per channel subunit). The activation of the voltage sensor precedes the opening of the central pore by 8 ms, and the voltage dependence of charge movement is 37 mV more negative than channel opening. The TRPP2 gating current is one-fourth the size of those measured from voltage-gated Na_v, Ca_v, and K_v channels. This is expected since TRPP2 has fewer gating charges than are found within typical VGIC voltage sensors (2 vs. 4 to 6 charges per voltage sensor). We demonstrate that preservation of both K3 and K4 gating charge positions is essential for the function of both TRPP2 and a typical VGIC, NaChBac. These results are supported by mutagenesis studies in the Shaker K_v channel, where the number of gating charges could not be reduced beyond positions K3 and K4 (49). With few exceptions, TRP channels do not have gating charges within their VSD. The cold-sensitive TRPM8 channel has a single positively charged residue at gating charge position K4 (44). While there is significant functional evidence that TRPM8 currents are voltage dependent, there are no reports of gating currents measured from TRPM8 channels. In addition, neutralizing the putative gating charge alters voltage and thermal sensitivity but does not abolish the ionic conductance entirely (50). Thus, it appears that TRPM8 can still function without a gating charge, an indication that its activation mechanism is different from that of TRPP2 and VGICs. In this study, we have shown that TRPP2 channels can be potentiated by osmotic membrane swelling and heat. However, these stimuli potentiate the TRPP2 current using distinct mechanisms. We find that membrane swelling reduces the membrane potential required to move the gating charge and enhances its open probability at negative membrane potentials. This is achieved by increasing the voltage sensitivity of the gating charges in the VSD. In contrast, heat enhances TRPP2 unitary ion conductance, a parameter controlled by the PD. Future work will be directed at a structural mechanism showing how the VSD activation integrates the membrane tension to alter TRPP2's voltage-dependent activation. Importantly, all polymodal means of activating TRPP2 fail to open the channel when 1 of the gating charges is neutralized.

State-Dependent Interactions and Structural Changes Within the VSD. A major thermodynamic obstacle to channel activation is the stabilization of gating charges within the hydrophobic core of the 4-helix bundle of the VSD. In VGICs, the gating charges form sequential ion pairs with anionic centers (An1 and An2), which are formed by glutamate and aspartate side chains of the S1 to S3 segments (4, 12). Here ion pairing with the anionic centers serves to stabilize the positive charge movement in a low dielectric constant environment of the membrane and catalyze this S4 segments transition. In VGICs, An1 forms an external coordination site for K1 and K2; however, these sites are not conserved in polycystin channels (F359 in TRPP2; *SI Appendix*, Fig. S1*B*). An2 forms an internal salt bridge with K3 or K4 in the deactivated and partially activated VGIC states (3, 4, 51). However, the side chain densities of An2 (D390), K3 and K4 are unresolved in the existing cryo-EM structures (20, 26–28). To address this gap, we used Rosetta to model the gating charge interactions in conjunction with mutant cycle analysis to test their energy of interaction. From the model, the K4 ammonium side chain clearly forms a salt bridge with carboxylate side chain of An2 (D390) in the closed state of TRPP2. As discussed previously, TRPP1 forms an ion channel in the primary cilia of the kidney collecting duct, and variants in TRPP1 cause autosomal polycystic kidney disease. The An2 variant D511V was shown to cause a complete loss of TRPP1 function when it was reconstituted from ER membranes into artificial bilayers (22). Here we demonstrate that substitutions of the gating charges or An2 rendered TRPP2 channels inactive as no TRPP2 current could be measured. Evidently, An2 interactions with these gating charges are essential for the opening of TRPP1 and TRPP2 channels, which are likely disrupted by nonsense and missense variants found within the VSD of TRPP1 that are associated with ADPKD (http://pkdb.mayo.edu/) (52).

In VGICs, the high number of gating charges hydrates the intracellular and extracellular clefts within the VSD and causes the electric field to focus across a 4-Å-wide cluster of hydrophobic residues (53). This results in ion channels that are steeply voltage dependent and open at negative membrane potentials (53, 54). By comparison, the VSD of TRPP2 has fewer gating charges and has a wider (7 Å) hydrophobic septum, features which likely contributes to its positive ($V_{1/2}$) and shallow (Z) voltage dependence. Based on our model, we report that S2 residue Y366 sequentially interacts with K3 in the deactivated state and with K4 in the activated state and that these interacting pairs are energetically coupled during channel opening. Since TRPP2 function was only preserved with a phenylalanine substitution at Y366 and not from hydrogen bond donor substations, we propose that it forms cation–π interactions with the gating charges. In K_v channels, the analogous aromatic residue to Y366 (F233 in Shaker) forms a gating charge transfer center that separates the aqueous extracellular from the intracellular lumens of the VSD and forms cation–π interactions with the gating charges (55). Using accessibility experiments, we determined that a cysteine at position H404 becomes exposed to the aqueous extracellular environment in the activated state. MTSES chemical modification of this site abolishes the gating current. We propose 2 possible explanations for these observations: either the negative charge modification at H404C neutralizes the positive gating charge transfer or it may impair the movement of the voltage sensor, perhaps trapping it in the activated or deactivated state(s). Since the charge state of H404 can influence channel gating, future experiments should determine if this site is responsible for proton and lipid modulation of current (25, 29). In addition, developing small molecules or biologics that target the VSD may provide useful research tools to study polycystin channels and may principally represent a therapeutic strategy to regulate TRPP1 function for the treatment of ADPKD.

Physiological Impact of Voltage-Dependent Modulation by Polymodal Stimuli. In this manuscript we demonstrate that osmotic membrane swell acts as a modifier of TRPP2's intrinsic voltage sensitivity. What is the physiological purpose of this modulation? The answer likely resides in the cellular and tissue-specific localization of polycystin channels. Channels containing heteromeric or homomeric versions of TRPP1 (TRPP1 + polycystin-1) and TRPP2 (TRPP2 + polycystin-1L1) are found in the cilia, plasma membrane, and ER membranes of epithelial cells of disparate organ systems. Epithelial cells carry out secretion, selective absorption, and sensory functions in organ systems. Since they interface inside cavities and lumen of organs, the membrane and cilia of these cells inevitably face osmotic changes which are unlike interstitial fluid conditions. For example, TRPP1 is found in the primary cilia and ER membranes kidney collecting duct principle cells—the last portion of the nephron responsible for the reabsorption of water to concentrate urine before excretion (19). These cells must adjust their intracellular tonicity to match that of the urine, which can oscillate between 200 and 1200 mOs/L under normal human diurnal conditions (56). When urine shifts from hypertonic to hypotonic salt conditions, water moves through aquaporin channels into the cell, which would dilute intracellular calcium levels. Here osmotic membrane swelling increases TRPP1 open times and may replenish calcium and monovalent ions to their basal intracellular concentrations. Thus, swell-induced opening of TRPP1 may have a calcium-homeostatic function in keeping the kidney collecting duct cells isotonic with the urine and maintaining a constant resting internal Ca^{2+} concentration during these normal physiological shifts in urine osmolarity. In addition to epithelial cells, TRPP2 is also expressed in the plasma membrane and ciliary membrane of excitable cells like cerebrospinal fluid contacting neurons (CSF-cNs) and type 3 taste receptor cells (TRCs) (38, 39, 57). Although 1% of our CSF is exchanged every minute, it is unclear if osmotic changes occur during this process (58). However, the CSF is under 10 to 15 mmHg of basal pressure and cells which interface the CSF experience pulsatile flow changes that are synchronized to the systolic blood pressure changes in the choroidal arteries (59). Opening of TRPP2 channels is enhanced at high pressure (>40 mmHg), and since both osmotic swell and pressure exert mechanical force on the membrane, it is possible that these pulsatile pressure changes may modulate the voltage dependence of TRPP2 channels in CSF-cNs of the spinal cord. Although the mechanism was not determined here, TRPP2 channels are also reported to be activated by acidic and alkaline pH. This modulation might not be physiologically relevant for these neurons because the CSF pH is tightly maintained. Nonetheless, in taste reception, where external pH is extreme, lingual TRCs express a heteromeric TRPP2 + polycystin-1L3 channels that contribute to the acid-evoked nerve response (38). Since pH alters the ionic voltage sensitivity of several divergent VGICs, it is possible that pH levels may modulate TRPP2 through protonation of the VSD (60–63).

The Evolutionary Relationship Between TRPP and VGIC VSDs. The polycystin channels diverged from primitive voltage-gated calcium channels and are oldest within the TRP family. They are found in simple eukaryotes like yeast, yet little is known about their physiological role in single-cell organisms (64, 65). In this study, we have compared the biophysical properties of TRPP2 and VGICs which share similar structural and functional features that control their conducting states. Over time, a common ancestor of polycystins must have evolutionarily segregated from the canonical VGICs and developed distinguishable traits, possibly to fill new physiological roles for these early eukaryotes. The hypothesis is similar to how Na_v was evolved as a result of evolutionary diversification from the ancestral Ca_v to adapt to a faster communication process in primitive multicellular organisms and to maintain osmotic balance in environments where salinity shifts (1). In the case of Ca_V to Na_V, their divergence began in the selectivity filter and is preserved in choanoflagellates, whose Na_V channel permeates Na^+ and Ca^{2+} ions (66, 67). In the case of TRPP channels, a major exaptation is the loss of nonessential gating charges, effectively causing the voltage dependence to shift to more positive potentials and preventing the channels from overfiring. We believe the VSD of TRPP2 has evolved to preclude the readdition of gating charges at positions K1 and K2, which cause a loss of function in our mutagenesis studies. Reasons for this are that outermost anionic countercharge center (An1) is replaced by bulky hydrophobic residues, which would limit the translation of the S4 during gating. Having a shallow and positive voltage dependence might be advantageous for selectively opening the channel under specific cellular conditions. For example, TRPP1 and TRPP2 channels function in primary cilia, which has a less negative membrane potential (−18 mV) compared with the plasma membrane (−53 mV) (68). Therefore, these channels are more likely to be opened in the ciliary compartment than on the membrane. Polycystin channel activation is polymodal, where voltage ultimately keeps the channel closed until stimuli—such as membrane swelling or elevated intracellular calcium—lowers the energetics of VSD activation to open the channel.

Materials and Methods

The experimental methods used to generate the presented data are summarized below, and a complete description of the can be found in *SI Appendix*. Unless otherwise indicated, all whole-cell electrophysiology experiments were performed in in symmetrical sodium. HEK 293T cells were transiently transfected (Lipofectamine 2000; Invitrogen) with the mammalian cell expression plasmid pTracer CMV2 containing the human PKD2-L1 gene (isoform 1) or with the pEGFP-N1 plasmid (Addgene) containing the *Bacillus* hallodurans voltage-gated sodium channel, NaChBac. SF9 cells expressing the PKD2L1 were generated using the Bac-to-bac TOPO expression system (Invitrogen). Live SF9 cells

expressing HA-PKD2L1-GFP and HEK cells expressing NaChBac-GFP were imaged using a Nikon A1 confocal microscope using a 40× objective 36 to 48 h after infection (SF9 cells) or transfection (HEK cells). Statistical significance was determined using Anova corrected for multiple comparisons with Dunette and unpaired Student's *t* tests. Rosetta structural modeling was performed using the cryo-EM structures of TRPP1 (Protein Data Bank [PDB] ID 5T4D) (20) and TRPP2 (PDB ID 5Z1W) (26) as templates to predict the TRPP2 structures in closed and open states, respectively.

ACKNOWLEDGMENTS. The work reported in this paper was supported by the Carl W. Gottschalk Research Scholar Grant from the American Society of Nephrology (ASN) and the ASN Foundation for Kidney Research, Mayo Clinic Robert M. and Billie Kelley Pirnie Translational PKD Research Center (National Institute of Diabetes and Digestive and Kidney Disease [NIDDK] P30 DK090728), Polycystic Kidney Disease Foundation research grant, Northwestern University Center for Kidney Research and Therapeutics research grant (NU Go KIDNEY), and NIDDK R00DK106655 and R56DK119709 to P.G.D.

1. B. Hille, *Ion Channels of Excitable Membranes* (Sinauer, Sunderland, MA, ed. 3, 2001), p. xviii, 814 pp.
2. W. Wang, R. MacKinnon, Cryo-EM structure of the open human ether-a-go-go-related K(+) channel hERG. *Cell* **169**, 422–430.e10 (2017).
3. S. B. Long, E. B. Campbell, R. Mackinnon, Crystal structure of a mammalian voltage-dependent Shaker family K+ channel. *Science* **309**, 897–903 (2005).
4. J. Payandeh, T. Scheuer, N. Zheng, W. A. Catterall, The crystal structure of a voltage-gated sodium channel. *Nature* **475**, 353–358 (2011).
5. E. Perozo, R. MacKinnon, F. Bezanilla, E. Stefani, Gating currents from a non-conducting mutant reveal open-closed conformations in Shaker K+ channels. *Neuron* **11**, 353–358 (1993).
6. C. M. Armstrong, F. Bezanilla, Currents related to movement of the gating particles of the sodium channels. *Nature* **242**, 459–461 (1973).
7. A. Sula *et al*., The complete structure of an activated open sodium channel. *Nat. Commun.* **8**, 14205 (2017).
8. L. Hofmann *et al*., The S4—S5 linker–Gearbox of TRP channel gating. *Cell Calcium* **67**, 156–165 (2017).
9. O. Yifrach, R. MacKinnon, Energetics of pore opening in a voltage-gated K(+) channel. *Cell* **111**, 231–239 (2002).
10. S. K. Aggarwal, R. MacKinnon, Contribution of the S4 segment to gating charge in the Shaker K+ channel. *Neuron* **16**, 1169–1177 (1996).
11. E. Vargas *et al*., An emerging consensus on voltage-dependent gating from computational modeling and molecular dynamics simulations. *J. Gen. Physiol.* **140**, 587–594 (2012).
12. V. Yarov-Yarovoy *et al*., Structural basis for gating charge movement in the voltage sensor of a sodium channel. *Proc. Natl. Acad. Sci. U.S.A.* **109**, E93–E102 (2012).
13. P. G. DeCaen, V. Yarov-Yarovoy, E. M. Sharp, T. Scheuer, W. A. Catterall, Sequential formation of ion pairs during activation of a sodium channel voltage sensor. *Proc. Natl. Acad. Sci. U.S.A.* **106**, 22498–22503 (2009).
14. I. S. Ramsey, M. Delling, D. E. Clapham, An introduction to TRP channels. *Annu. Rev. Physiol.* **68**, 619–647 (2006).
15. K. Venkatachalam, C. Montell, TRP channels. *Annu. Rev. Biochem.* **76**, 387–417 (2007).
16. C. Montell The TRP superfamily of cation channels. *Sci. STKE* **2005**, re3 (2005).
17. T. Voets, A. Janssens, J. Prenen, G. Droogmans, B. Nilius, Mg2+-dependent gating and strong inward rectification of the cation channel TRPV6. *J. Gen. Physiol.* **121**, 245–260 (2003).
18. W. L. Wei *et al*., TRPM7 channels in hippocampal neurons detect levels of extracellular divalent cations. *Proc. Natl. Acad. Sci. U.S.A.* **104**, 16323–16328 (2007).
19. C. Bergmann *et al*., Polycystic kidney disease. *Nat. Rev. Dis. Primers* **4**, 50 (2018).
20. P. S. Shen *et al*., The structure of the polycystic kidney disease channel PKD2 in lipid nanodiscs. *Cell* **167**, 763–773.e11 (2016).
21. X. Liu *et al*., Polycystin-2 is an essential ion channel subunit in the primary cilium of the renal collecting duct epithelium. *eLife* **7**, e33183 (2018).
22. P. Koulen *et al*., Polycystin-2 is an intracellular calcium release channel. *Nat. Cell Biol.* **4**, 191–197 (2002).
23. S. J. Kleene, N. K. Kleene, The native TRPP2-dependent channel of murine renal primary cilia. *Am. J. Physiol. Renal. Physiol.* **312**, F96–F108 (2017).
24. P. G. DeCaen, M. Delling, T. N. Vien, D. E. Clapham, Direct recording and molecular identification of the calcium channel of primary cilia. *Nature* **504**, 315–318 (2013).
25. M. Wilkes *et al*., Molecular insights into lipid-assisted Ca^{2+} regulation of the TRP channel Polycystin-2. *Nat. Struct. Mol. Biol.* **24**, 123–130 (2017).
26. Q. Su *et al*., Cryo-EM structure of the polycystic kidney disease-like channel PKD2L1. *Nat. Commun.* **9**, 1192 (2018).
27. R. E. Hulse, Z. Li, R. K. Huang, J. Zhang, D. E. Clapham, Cryo-EM structure of the polycystin 2-l1 ion channel. *eLife* **7**, e36931 (2018).
28. M. Grieben *et al*., Structure of the polycystic kidney disease TRP channel Polycystin-2 (PC2). *Nat. Struct. Mol. Biol.* **24**, 114–122 (2017).
29. T. Shimizu, A. Janssens, T. Voets, B. Nilius, Regulation of the murine TRPP3 channel by voltage, pH, and changes in cell volume. *Pflugers Arch.* **457**, 795–807 (2009).
30. T. Numata *et al*., Integrative approach with electrophysiological and theoretical methods reveals a new role of S4 positively charged residues in PKD2L1 channel voltage-sensing. *Sci. Rep.* **7**, 9760 (2017).
31. P. G. DeCaen, X. Liu, S. Abiria, D. E. Clapham, Atypical calcium regulation of the PKD2-L1 polycystin ion channel. *eLife* **5**, e13413 (2016).
32. A. Kuzmenkin, F. Bezanilla, A. M. Correa, Gating of the bacterial sodium channel, NaChBac: Voltage-dependent charge movement and gating currents. *J. Gen. Physiol.* **124**, 349–356 (2004).
33. D. Ren *et al*., A prokaryotic voltage-gated sodium channel. *Science* **294**, 2372–2375 (2001).
34. D. Sigg, F. Bezanilla, Total charge movement per channel. The relation between gating charge displacement and the voltage sensitivity of activation. *J. Gen. Physiol.* **109**, 27–39 (1997).
35. N. E. Schoppa, K. McCormack, M. A. Tanouye, F. J. Sigworth, The size of gating charge in wild-type and mutant Shaker potassium channels. *Science* **255**, 1712–1715 (1992).
36. F. Bezanilla, E. Perozo, D. M. Papazian, E. Stefani, Molecular basis of gating charge immobilization in Shaker potassium channels. *Science* **254**, 679–683 (1991).
37. I. G. Ishida, G. E. Rangel-Yescas, J. Carrasco-Zanini, L. D. Islas, Voltage-dependent gating and gating charge measurements in the Kv1.2 potassium channel. *J. Gen. Physiol.* **145**, 345–358 (2015).
38. A. L. Huang *et al*., The cells and logic for mammalian sour taste detection. *Nature* **442**, 934–938 (2006).
39. A. Orts-Del'Immagine *et al*., A single polycystic kidney disease 2-like 1 channel opening acts as a spike generator in cerebrospinal fluid-contacting neurons of adult mouse brainstem. *Neuropharmacology* **101**, 549–565 (2016).
40. T. Higuchi, T. Shimizu, T. Fujii, B. Nilius, H. Sakai, Gating modulation by heat of the polycystin transient receptor potential channel PKD2L1 (TRPP3). *Pflugers Arch.* **466**, 1933–1940 (2014).
41. S. Zhang, N. Li, W. Zeng, N. Gao, M. Yang, Cryo-EM structures of the mammalian endo-lysosomal TRPML1 channel elucidate the combined regulation mechanism. *Protein Cell* **8**, 834–847 (2017).
42. M. Liao, E. Cao, D. Julius, Y. Cheng, Structure of the TRPV1 ion channel determined by electron cryo-microscopy. *Nature* **504**, 107–112 (2013).
43. F. Yang, J. Zheng, Understand spiciness: Mechanism of TRPV1 channel activation by capsaicin. *Protein Cell* **8**, 169–177 (2017).
44. Y. Yin *et al*., Structure of the cold- and menthol-sensing ion channel TRPM8. *Science* **359**, 237–241 (2018).
45. A. Samanta, J. Kiselar, R. A. Pumroy, S. Han, V. Y. Moiseenkova-Bell, Structural insights into the molecular mechanism of mouse TRPA1 activation and inhibition. *J. Gen. Physiol.* **150**, 751–762 (2018).
46. F. Bezanilla, The voltage sensor in voltage-dependent ion channels. *Physiol. Rev.* **80**, 555–592 (2000).
47. W. A. Catterall, Molecular properties of voltage-sensitive sodium channels. *Annu. Rev. Biochem.* **55**, 953–985 (1986).
48. D. M. Starace, F. Bezanilla, Histidine scanning mutagenesis of basic residues of the S4 segment of the shaker k+ channel. *J. Gen. Physiol.* **117**, 469–490 (2001).
49. Y. Xu, Y. Ramu, Z. Lu, A shaker K+ channel with a miniature engineered voltage sensor. *Cell* **142**, 580–589 (2010).
50. T. Voets, G. Owsianik, A. Janssens, K. Talavera, B. Nilius, TRPM8 voltage sensor mutants reveal a mechanism for integrating thermal and chemical stimuli. *Nat. Chem. Biol.* **3**, 174–182 (2007).
51. J. Payandeh, T. M. Gamal El-Din, T. Scheuer, N. Zheng, W. A. Catterall, Crystal structure of a voltage-gated sodium channel in two potentially inactivated states. *Nature* **486**, 135–139 (2012).
52. A. M. Gout, N. C. Martin, A. F. Brown, D. Ravine, PKDB: Polycystic Kidney Disease Mutation Database–A gene variant database for autosomal dominant polycystic kidney disease. *Hum. Mutat.* **28**, 654–659 (2007).
53. D. M. Starace, F. Bezanilla, A proton pore in a potassium channel voltage sensor reveals a focused electric field. *Nature* **427**, 548–553 (2004).
54. L. D. Islas, F. J. Sigworth, Electrostatics and the gating pore of Shaker potassium channels. *J. Gen. Physiol.* **117**, 69–89 (2001).
55. S. A. Pless, J. D. Galpin, A. P. Niciforovic, C. A. Ahern, Contributions of counter-charge in a potassium channel voltage-sensor domain. *Nat. Chem. Biol.* **7**, 617–623 (2011).
56. E. T. Perrier *et al*., Twenty-four-hour urine osmolality as a physiological index of adequate water intake. *Dis. Markers* **2015**, 231063 (2015).
57. E. Jalalvand *et al*., Cerebrospinal fluid-contacting neurons sense pH changes and motion in the hypothalamus. *J. Neurosci.* **38**, 7713–7724 (2018).
58. A. C. Guyton, J. E. Hall, *Textbook of Medical Physiology* (W.B. Saunders, Philadelphia, ed. 9, 1996), p. xliii, 1148 pp.
59. L. Sakka, G. Coll, J. Chazal, Anatomy and physiology of cerebrospinal fluid. *Eur. Ann. Otorhinolaryngol. Head Neck Dis.* **128**, 309–316 (2011).
60. A. Khan, J. W. Kyle, D. A. Hanck, G. M. Lipkind, H. A. Fozzard, Isoform-dependent interaction of voltage-gated sodium channels with protons. *J. Physiol.* **576**, 493–501 (2006).
61. C. H. Peters, M. R. Ghovanloo, C. Gershome, P. C. Ruben, pH modulation of voltage-gated sodium channels. *Handb. Exp. Pharmacol.* **246**, 147–160 (2018).
62. J. V. Steidl, A. J. Yool, Differential sensitivity of voltage-gated potassium channels Kv1.5 and Kv1.2 to acidic pH and molecular identification of pH sensor. *Mol. Pharmacol.* **55**, 812–820 (1999).
63. T. Cens, M. Rousset, P. Charnet, Two sets of amino acids of the domain I of Cav2.3 Ca(2+) channels contribute to their high sensitivity to extracellular protons. *Pflugers Arch.* **462**, 303–314 (2011).
64. X. L. Zhou *et al*., The transient receptor potential channel on the yeast vacuole is mechanosensitive. *Proc. Natl. Acad. Sci. U.S.A.* **100**, 7105–7110 (2003).
65. H. Matsuura, T. Sokabe, K. Kohno, M. Tominaga, T. Kadowaki, Evolutionary conservation and changes in insect TRP channels. *BMC Evol. Biol.* **9**, 228 (2009).
66. H. H. Zakon, Adaptive evolution of voltage-gated sodium channels: The first 800 million years. *Proc. Natl. Acad. Sci. U.S.A.* **109** (suppl. 1), 10619–10625 (2012).
67. B. J. Liebeskind, D. M. Hillis, H. H. Zakon, Evolution of sodium channels predates the origin of nervous systems in animals. *Proc. Natl. Acad. Sci. U.S.A.* **108**, 9154–9159 (2011).
68. M. Delling, P. G. DeCaen, J. F. Doerner, S. Febvay, D. E. Clapham, Primary cilia are specialized calcium signalling organelles. *Nature* **504**, 311–314 (2013).